Available online at www.sciencedirect.com
ScienceDirect
Journal of Power Sources 170 (2007) 61–66
JOURNAL OF POWER SOURCES
www.elsevier.com/locate/jpowsour

Short communication

$La(Ni,Fe)O_3$ as a cathode material with high tolerance to chromium poisoning for solid oxide fuel cells

Y.D. Zhen [a], A.I.Y. Tok [a,*], S.P. Jiang [b], F.Y.C. Boey [a]

[a] School of Materials Science and Engineering, Nanyang Technological University, 50 Nanyang Avenue, Singapore 639798, Singapore
[b] School of Mechanical and Aerospace Engineering, Nanyang Technological University, 50 Nanyang Avenue, Singapore 639798, Singapore

Received 15 January 2007; accepted 27 March 2007
Available online 20 April 2007

Abstract

A novel cathode material, $La(Ni_{0.4}Fe_{0.6})O_3$ (LNF), is synthesized by a solid-state reaction for applications in solid oxide fuel cells (SOFCs). The electrochemical performance of the LNF cathode is investigated for the oxygen reduction reaction at 900 °C in the presence of a Fe–Cr alloy interconnect, and compared with $(La,Sr)MnO_3$ (LSM) cathodes. Under these conditions, the LNF electrode has a more stable electrochemical activity than that of the LSM electrode. There is no deposition of chromium species on the electrode surface or at the LNF electrode|yttria-stabilized zirconia (YSZ) electrolyte interface after passage of 200 mA cm^{-2} for 20 h at 900 °C. By contrast, a significant amount of chromium species is preferentially deposited at the LSM|YSZ interface regions for the LSM electrode. The results demonstrate that the LNF electrode has high tolerance to chromium poisoning, and is, therefore, promising as a SOFC cathode when using chromia-forming alloy interconnects.

Keywords: LNF cathode; Chromuim poisoning; Solid oxide fuel cell; Metallic interconnect; Electro chemical performance; Chromia-forming alloy

1. Introduction

Intermediate-temperature solid oxide fuel cells (IT-SOFCs) have received much attention as an environmentally friendly and highly efficient power generation system with very low emissions of greenhouse gases. The lower operating temperature allows the use of metallic materials as the interconnects. The metals, especially the chromia-forming ferrite stainless steels, are preferred due to their high thermal and electronic conductivity, negligible ionic conductivity, good machineability and low material cost [1]. Neverthless, this application of chromia-forming alloys still poses many challenges even at reduced temperatures. For instance, the oxide scale formed on the surface of the alloy after long-time exposure in the SOFC environment results in high electrical resistance which degrades stack performance [2–4]. Furthermore, under high temperature volatile Cr species such as CrO_3 and $CrO_2(OH)_2$ are generated over the oxide scale layer in oxidizing atmospheres [5,6]. These species can cause rapid performance deterioration in the SOFC due to the poisoning of cathodes such as $(La,Sr)MnO_3$ (LSM) and $(La,Sr)(Co,Fe)O_3$ (LSCF) in the oxygen reduction reaction [7–11]. The poisoning is largely due to the deposition of Cr species at the electrode|electrolyte interface regions or on the electrolyte surface.

We have studied in detail the mechanism and kinetics of the deposition of Cr species at LSM and the LSCF electrodes under SOFC operation conditions [11–14]. It was found that the deposition process is essentially dominated by the chemical dissociation of the gaseous Cr species, and is most likely limited by the nucleation reaction these species and nucleation agents such as manganese species (Mn^{2+}) generated under cathodic polarization in LSM electrode–zirconia electrolyte system or SrO species enriched originally at the electrode surface in the LSCF electrode–ceria electrolyte system [10,12]. Systematic studies have shown that the interaction between the Cr species and electrodes is strongly dependent on the nature of the electrode and electrolyte materials [14]. This suggests the possibility to develop stable cathode materials with high tolerance to Cr poisoning by proper modification of the cathode composition, i.e., without a nucleation agent for Cr deposition.

$La(Ni,Fe)O_3$ perovskite material has been developed as one of most promising cathode materials for the IT-SOFCs because

* Corresponding author. Tel.: +65 67904935; fax: +65 67909081.
E-mail address: miytok@ntu.edu.sg (A.I.Y. Tok).

0378-7753/$ – see front matter © 2007 Elsevier B.V. All rights reserved.
doi:10.1016/j.jpowsour.2007.03.079

it has high electrochemical activity for the oxygen reduction reaction and a thermal expansion coefficient close to that of zirconia electrolyte [15–17]. There are, however, few reports of the interaction between the LNF cathode and the chromia-forming alloy interconnect. In this study, LNF is prepared as an alternative cathode for the metallic interconnect. The electrochemical performance of the cathode for oxygen reduction is investigated in the presence of Fe–Cr alloy interconnect. For comparison, the interaction between the Fe–Cr alloy interconnect and the traditional cathode, LSM, is also examined under the same conditions. Details of such interaction can be found in our previous publications [12,13].

2. Experimental

$La(Ni_{0.6}Fe_{0.4})O_3$ (LNF) and $(La_{0.8}Sr_{0.2})_{0.9}MnO_3$ (LSM) cathode powders were synthesized by a solid-state reaction. La_2O_3, NiO, Fe_2O_3, $SrCO_3$ and $MnCO_3$ powders of appropriate composition were ball-milled in isopropanal and then calcined at 950 and 900 °C in air to produce LNF and LSM powder, respectively. The X-ray diffraction (XRD) patterns of the LNF and LSM powders are shown in Fig. 1 and demonstrate a single perovskite phase.

Electrolyte discs were prepared from 8 mol% Y_2O_3-doped ZrO_2 powder (YSZ, Tosoh, Japan) by die-pressing, followed by sintering at 1500 °C for 4 h in air. The sintered electrolyte thickness and diameter were ~1 and 19 mm, respectively. Electrode inks were prepared by mixing the LNF or LSM powders with polyethylene glycol and were applied to the YSZ electrolyte by a screen-printing method. The LNF and LSM electrodes were then sintered at 1100 and 1150 °C for 2 h in air, respectively. The electrode thickness was ~30 μm and the electrode area was 0.5 cm^2. Platinum paste (Ferro Corporation, USA) was painted on the other side of the YSZ electrolyte substrate to serve as counter and reference electrodes. The counter electrode was symmetrical to the working electrode and the reference electrode was painted as a ring around the counter electrode. The gap between the counter and reference electrodes was ~4 mm. The platinum electrodes were sintered at 1000 °C for 1 h in air.

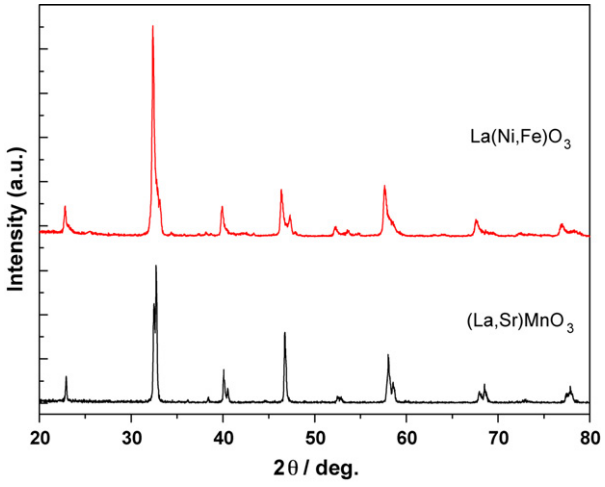

Fig. 1. XRD patterns of LNF and LSM powders.

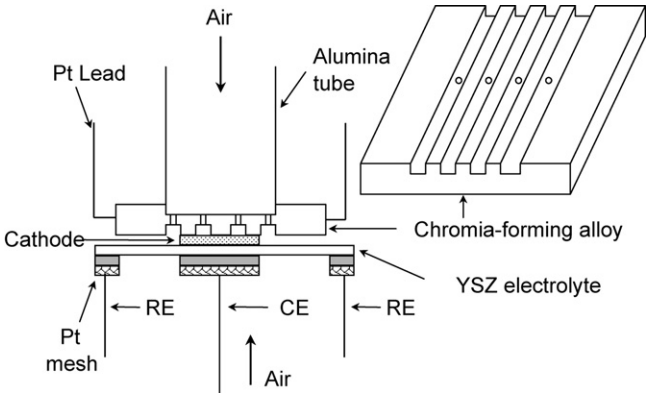

Fig. 2. Cell configuration and arrangement of the Fe–Cr alloy interconnect.

Iron–chromium alloy (RA446 with 23–27 wt.% Cr, 1.5 wt.% Mn, 1 wt.% Si, 0.2 wt.% C, 0.12 wt.% N and the remaining Fe, Rolled Alloy Co., Canada) was used as the interconnect. The alloys were machined into coupons (12 mm × 12 mm × 4 mm) with channels (1.2 mm × 1.2 mm) cut on one side of the coupon. Air was directed to the channels through an alumina tube. Two platinum wires were spot-welded to the alloy to serve as voltage and current probes, respectively. The interconnect was then placed directly on the LBCF electrode coating. The alloy also acted as a current-collector. Air (Industrial grade, H_2O content <3 ppm), after drying through a molecular sieve, was introduced at a flowing rate of 100 ml min^{-1}. The test cell arrangement in the presence of a Fe–Cr alloy interconnect is shown in Fig. 2. Details of the experimental set-up can also found in previous publications [11,14].

The initial electrochemical behaviour of LNF and LSM electrodes in the presence of a Fe–Cr alloy interconnect was examined under a constant current density of 200 mA cm^{-2} in air at 900 °C. The polarization potential ($E_{Cathode}$) was measured against the platinum|air reference electrode. The passage of current was interrupted from time to time to make electrochemical impedance spectroscopy (EIS) measurements. A Solartron 1260 frequency response analyzer in combination with a 1287 electrochemical interface was used for EIS measurements, with a frequency range of 100 kHz to 0.1 Hz and a signal amplitude of 10 mV. The EIS measurements were conducted at open-circuit. The electrode ohmic resistance (R_Ω) was measured from the high-frequency intercept and the electrode interface (polarization) resistance (R_E) was obtained from the difference between the high-frequency and the low-frequency intercepts on the impedance spectrum. The overpotential (η) was obtained from $E_{Cathode}$ and R_Ω ($\eta = E_{Cathode} - jR_\Omega$, where j is the current density).

Scanning electron microscopy (SEM, JEOL 6360, Japan) and X-ray energy dispersion spectroscopy (EDS, Oxford, UK) were used to examine the electrode morphology and the elemental distribution, respectively. In order to view the YSZ electrolyte surface in contact with the electrode, the electrode coating was removed by 20% HCl acid treatment and washing in de-ionized water.

3. Results and discussion

The initial impedance responses of the LSM and LNF electrodes for oxygen reduction under a cathodic current of 200 mA cm^{-2} at 900 °C in the presence of Fe–Cr alloy interconnect are shown in Fig. 3. For the reaction on the LSM electrode, the initial impedance before the passage of cathodic current is characterized by a large and depressed arc and the overall electrode polarization resistance (R_E) is 4.04 Ω cm^2. With the passage of current, the impedance arcs are reduced significantly. After 10 min, R_E is reduced to 0.87 Ω cm^2, i.e., to much smaller than the initial value, and this demonstrates the activation effects of cathodic current treatment on the electrochemical activity of the LSM electrode for oxygen reduction [17–21]. Similarly, the impedance arcs for oxygen reduction on the LNF electrode at 900 °C change with passage of cathodic current. The initial R_E is 5.13 Ω cm^2 and reduces to 3.43 Ω cm^2 after 240 min. The activation effect of cathodic current treatment on the electrochemical performance of a freshly prepared LNF electrode is also observed for oxygen reduction in the absence of Fe–Cr alloy. Orui et al. [16] proposed that the activation effect is propably related to a morphological change of the LNF electrode and the LNF electrode|zirconia electrolyte interfacial microstructure during current passage. The mechanisms by which cathodic polarization enhances the performance are still not clear.

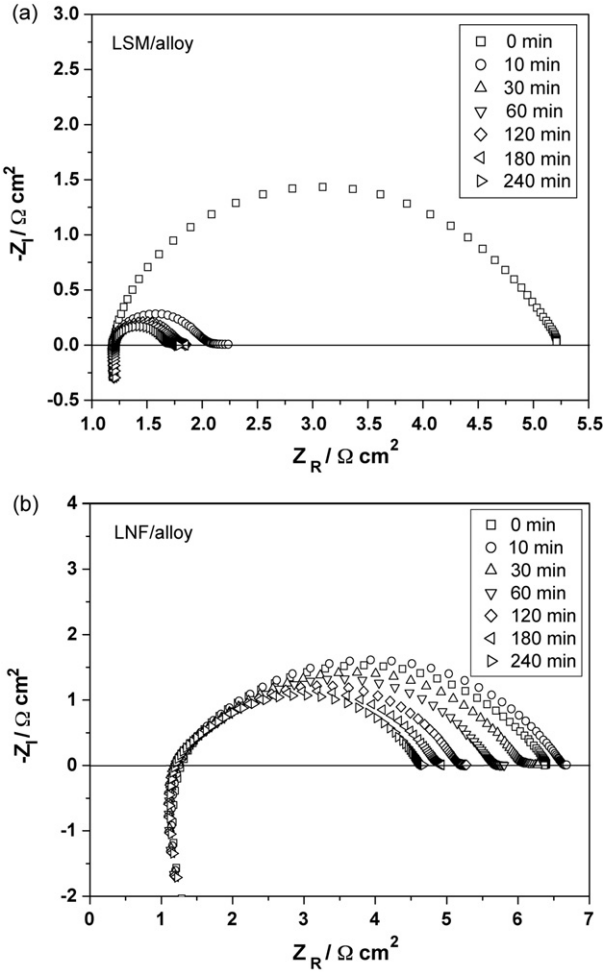

Fig. 3. Initial impedance responses of (a) LSM and (b) LNF electrodes as function of cathodic current passage time at 200 mA cm^{-2} and 900 °C in presence of Fe–Cr alloy interconnect.

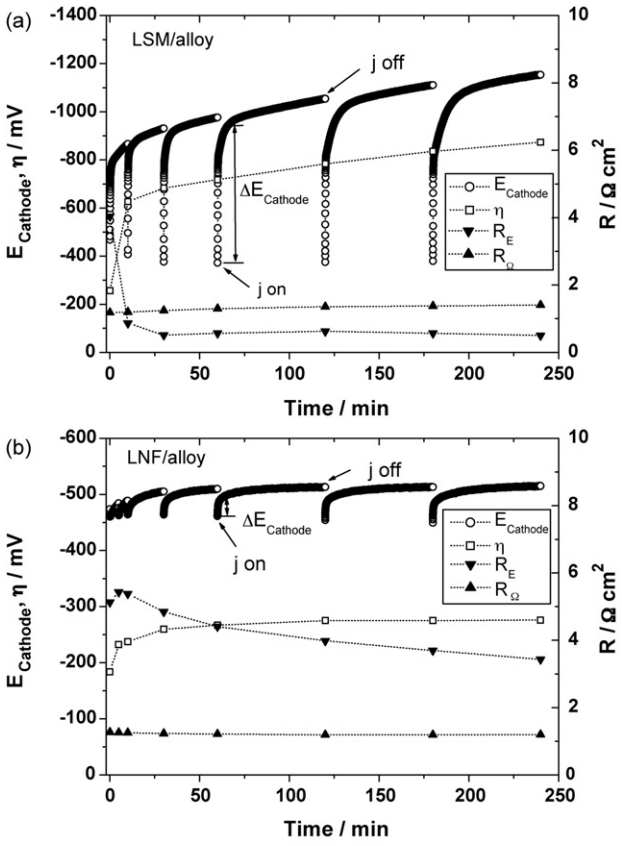

Fig. 4. Polarization curves of (a) LSM and (b) LNF electrodes as function of the cathodic current passage time at 200 mA cm^{-2} and 900 °C in presence of Fe–Cr alloy interconnect.

The initial polarization curves of the LSM and LNF electrodes as a function of the passage of cathodic current at 200 mA cm^{-2} and 900 °C in the presence of a Fe–Cr alloy interconnect are given in Fig. 4. For oxygen reduction on the LSM electrode, the polarization potential ($E_{Cathode}$) increases rapidly initially and reaches a potential region where the incease in $E_{Cathode}$ is much slower. The change in $E_{Cathode}$ is almost fully reproducible during the early stage of the polarization. Such time behaviour of $E_{Cathode}$ is exactly opposite to that in the absence of Fe–Cr alloy, which indicates the significant poisoning effect of the gaseous Cr species on oxygen reduction at the LSM electrode [11,22]. The increase in polarization potential is due mainly to an increase in overpotential (η), as the electrode ohmic resistance (R_Ω) remains almost constant. Similarly, the polarization potential for oxygen reduction on the LNF electrode in the presence of Fe–Cr alloy also develops two distinct potential regions. Nevertheless, the magnitude of the $E_{Cathode}$ increase (i.e., $\Delta E_{Cathode}$ as shown in Fig. 4) for the reaction on the LNF electrode is much smaller than that on the LSM electrode. For example, after passing current for 120 min, $\Delta E_{Cathode}$ is ~55 mV for the LNF electrode and ~656 mV for the LSM electrode. The much smaller value on the LNF electrode in the presence of Fe–Cr

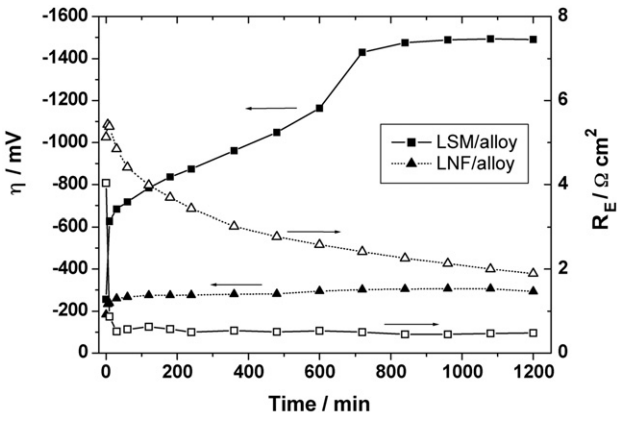

Fig. 5. Plots of overpotential (η) and polarization resistance (R_E) as function of cathodic current passage time at 200 mA cm^{-2} and 900 °C in presence of Fe–Cr alloy interconnect.

alloy shows the less inhibiting effect of gaseous Cr species on the kinetics of oxygen reduction.

The change in overpotential and polarization resistance is shown in Fig. 5 as a function of current passage time for O_2 reduction on LSM and LNF electrodes in the presence of Fe–Cr alloy for 20 h at 900 °C. For both electrodes, R_E decreases. This is also an indication that Cr deposition is not dominated by the electrochemical deposition of gaseous Cr species in competition with oxygen reduction at the three-phase boundary, as proposed earlier [12,13]. On the other hand, at the end of 20 h the overpotential (η) increases from 256 to 1490 mV for reaction on the LSM electrode. For the LNF electrode, the initial η is 253 mV and increases to 307 mV after 20 h. The increase in η is much smaller than that on the LSM electrode. Thus, the deterioration of the electrode performance caused by Cr species is substantially smaller for the LNF electrode. This clearly shows that the LNF electrode has much higher tolerance towards the gaseous Cr species.

Scanning electron micrographs of the surface and fractured cross-section of the LNF and LSM electrodes are shown in Fig. 6 and were obtained after cathodic current passage at 200 mA cm^{-2} and 900 °C for 20 h in the presence of a Fe–Cr alloy interconnect. The microstructure of the LNF electrode is characterized by uniformly distributed LSCF particles with a grain size of ~0.5 μm (Fig. 5(a)). There is also a good distribution of large and small pores. In general, the surface of the LNF electrode is very clean with no visible Cr deposition. EDS analysis shows no Cr on the electrode surface. Meanwhile, there is no visible deposition of Cr species at the LNF|YSZ interface, as shown in Fig. 6(b). Similarly, no Cr is found on the LSM electrode surface (Fig. 6(c)). The granular-shaped particles are pure LSM particles, the size of which is in the range of 0.8–2.5 μm. There is, however, significant deposition of Cr species at the LSM|YSZ interface, as shown by the formation of well-defined crystals with distinct facets at the interface (Fig. 6(d)). The deposition of Cr species preferentially occurs on the YSZ electrolyte surface at the electrolyte|electrode surface for the reaction at the LSM electrode.

To reveal the YSZ electrolyte surface in contact with the electrode coating, the LNF and the LSM electrode coatings

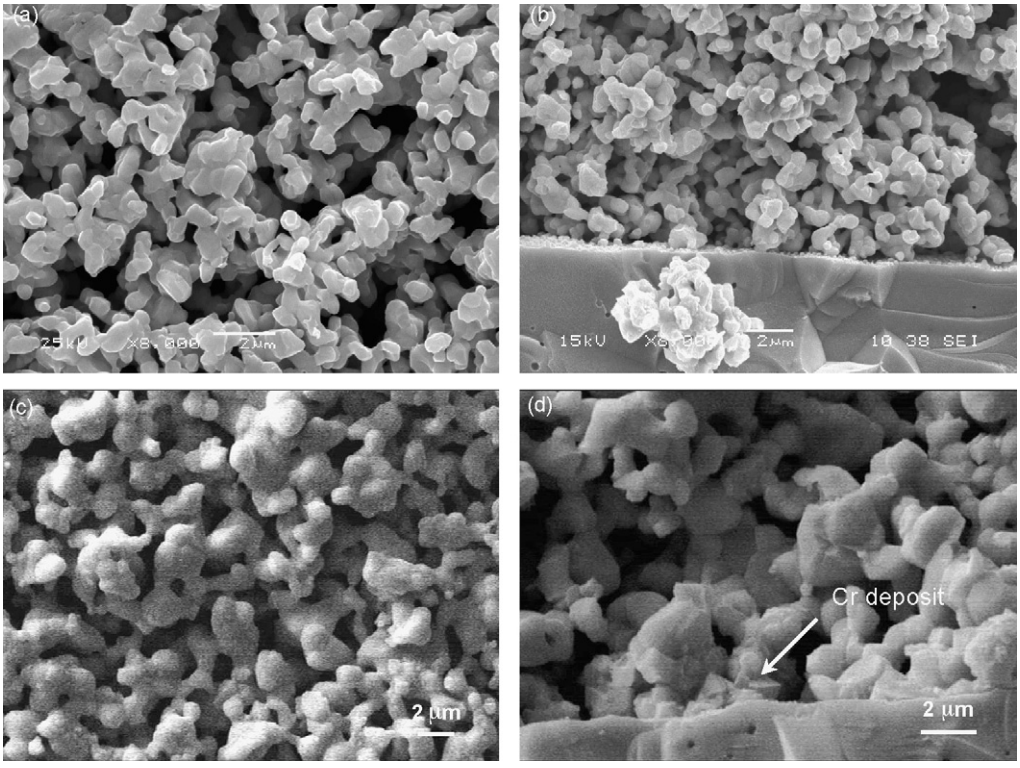

Fig. 6. SEM micrographs of (a) surface, (b) cross-section of LNF, (c) surface and (d) cross-section of LSM electrode after cathodic current passage at 200 mA cm^{-2} and 900 °C for 20 h.

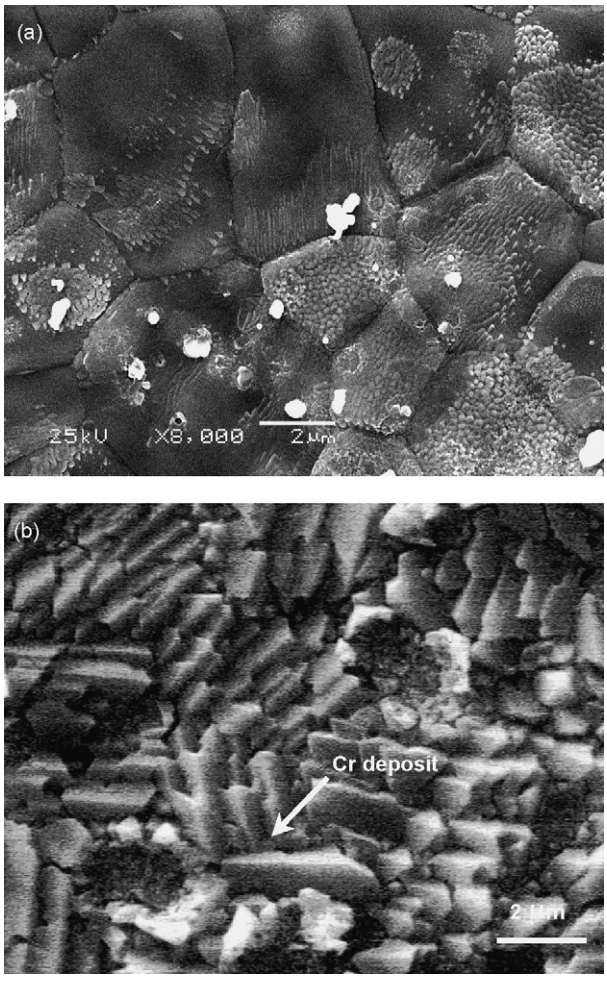

Fig. 7. SEM micrographs of YSZ electrolyte surface in contact with (a) LNF and (b) LSM electrodes after cathodic polarization for 20 h. Electrode coating removed by HCl acid treatment.

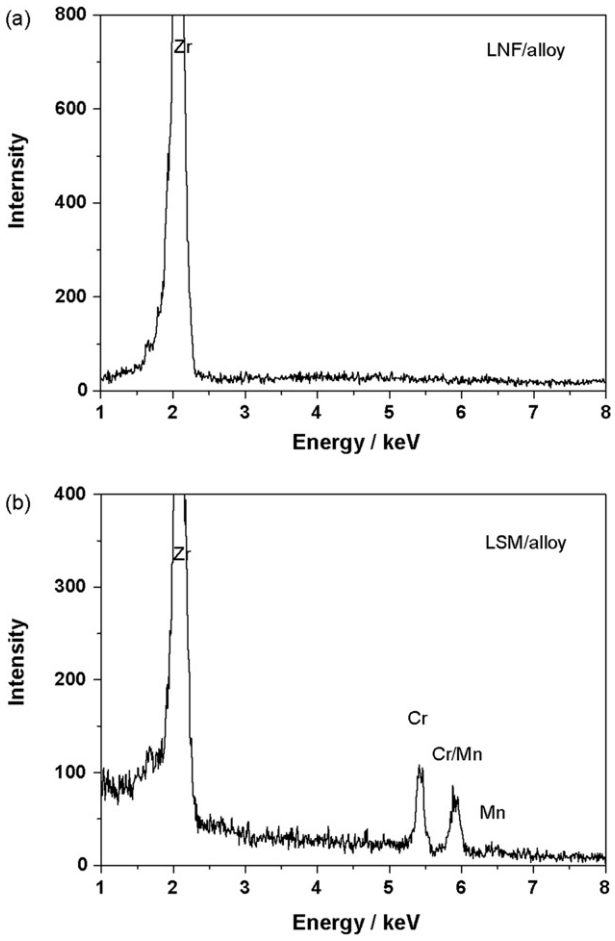

Fig. 8. EDS patterns of particles on YSZ electrolyte surface of Fig. 7: (a) LNF and (b) LSM electrodes.

were removed by HCl acid treatment, as shown in Fig. 7. The corresponding EDS patterns of the particles remaining on the electrolyte surface are shown in Fig. 8. For the LSM electrode, the YSZ electrolyte surface is almost completely covered by large crystals (~0.8–2 μm), which have distinct facets. EDS analysis of the crystals reveals the existence of Cr and Mn (Fig. 8(b)), which indicates the formation of $(Cr,Mn)_3O_4$ spinels [12]. With the LNF electrode, however, the YSZ electrolyte surface is much cleaner without deposition of Cr species, as shown by the clear boundaries of the YSZ grains. No Cr was detected by EDS analysis (Fig. 8(a)). The irregular particles at the YSZ electrolyte surface are most likely $La_2Zr_2O_7$ formed during the sintering step. Chiba et al. [15] and Orui et al. [16] reported that the stoichiometric LNF reacts with the zirconia electrolyte to form a $La_2Zr_2O_7$ layer at the LNF|YSZ electrolyte interface when the sintering temperature exceeds 1000 °C, which is lower than that used in this study. Obviously, the SEM observation shows that the deposition of Cr species is much less for the reaction on the LNF electrode as compared with that on the LSM electrode. The Cr species at the LNF electrode is no longer preferred on the YSZ electrolyte surface.

As shown in earlier studies [12,13], interaction between the Fe–Cr alloy interconnect and the LSM electrode will lead to significant deposition of Cr species at the YSZ interface and the formation of fine Cr_2O_3 grains and large $(Cr,Mn)_3O_4$ spinels. There is negligible Cr deposition inside the bulk of the LSM electrode or on the electrode surface during the early stage of the reaction. The deposition of Cr species is a chemical reaction in nature. It is kinetically controlled by a nucleation reaction between the gaseous Cr species and Mn^{2+} species generated under the cathodic polarization. In this study, however, under the same testing conditions, there is no visible Cr deposition on the LNF electrode surface or at the LNF|YSZ interface (Figs. 6 and 7). The deposition of Cr species on the LNF electrode is much smaller than that on the LSCF electrode. The results clearly indicate that the nucleation/grain growth for deposition of Cr species is kinetically inhibited or reduced for the reaction on the LNF electrode, i.e., the latter is more chemically stable towards Cr poisoning. This is in agreement with the more stable electrochemical performance of the LNF electrode for oxygen reduction in the presence of a Fe–Cr alloy interconnect. As shown in previous studies of a LSM electrode [22,23], Cr deposits on the electrolyte surface strongly inhibit the process of oxygen migration and incorporation into the electrolyte and this results in rapid degradation of performance. The much

cleaner electrode/electrolyte surface for the reaction on the LNF electrode illustrates that the inhibiting effect of Cr deposits on the oxygen migration and diffusion process will be substantially smaller in comparison with that on the LSM electrode. This explains the stable electrochemical performance of the LNF in the presence of Fe–Cr alloy (Fig. 5). The results in this study clearly demonstrate that the LNF electrode not only shows stable activity for oxygen reduction, but also significantly inhibits the deposition of Cr species.

4. Conclusion

The interaction and performance of a LNF electrode in the presence of a Fe–Cr alloy interconnect have been studied at 900 °C. The LNF shows a stable electrochemical performance in the presence of a Fe–Cr alloy interconnect. The degradation in performance is much smaller in comparison with the reaction on the LSM electrode. Scanning election micrographs show that the deposition of Cr species on the LNF electrode is very small. The results demonstrate that the LNF electrode has a high tolerance to Cr positioning. This indicates that LNF is a promising material for an intermediate-temperature SOFC cathode when a chromia-forming alloy is used for the interconnect in SOFCs.

References

[1] J.W. Fergus, Mater. Sci. Eng. A 397 (2005) 271.
[2] W.Z. Zhu, S.C. Deevi, Mater. Res. Bull. 38 (2003) 957.
[3] K. Huang, P.Y. Hou, J.B. Goodenough, Solid-State Ionics 129 (2000) 237.
[4] Z. Yang, K.S. Weil, D.M. Paxton, J.W. Stevenson, J. Electrochem. Soc. 150 (2003) A1188.
[5] H.G. Graham, H.H. Davis, J. Am. Ceram. Soc. 54 (1971) 89.
[6] K. Hilpert, D. Das, M. Miller, D.H. Peck, R. Weiβ, J. Electrochem. Soc. 143 (1996) 3642.
[7] S. Taniguchi, M. Kadowaki, H. Kawamura, T. Yasuo, Y. Akiyama, Y. Miyake, T. Saitoh, J. Power Sources 55 (1995) 73.
[8] S.P.S. Badwal, R. Deller, K. Foger, Y. Ramprakash, J.P. Zhang, Solid-State Ionics 99 (1997) 297.
[9] S.C. Paulson, V.I. Birss, J. Electrochem. Soc. 151 (2004) A1961.
[10] S.P. Jiang, S. Zhang, Y.D. Zhen, J. Electrochem. Soc. 153 (2006) A127.
[11] S.P. Jiang, J.P. Zhang, K. Foger, J. Electrochem. Soc. 147 (2000) 3195.
[12] S.P. Jiang, J.P. Zhang, L. Apateanu, K. Foger, J. Electrochem. Soc. 147 (2000) 4013.
[13] S.P. Jiang, S. Zhang, Y.D. Zhen, J. Mater. Res. 20 (2005) 747.
[14] S.P. Jiang, J.P. Zhang, X.G. Zheng, J. Euro. Ceram. Soc. 22 (2002) 361.
[15] R. Chiba, F. Yoshimura, Y. Sakurai, Solid-State Ionics 124 (1999) 281.
[16] H. Orui, K. Watanabe, R. Chiba, M. Arakawa, J. Electrochem. Soc. 151 (2004) A1412.
[17] S. Li, J. Sun, X. Sun, B. Zhu, Electrochem. Solid-State Lett. 9 (2006) A86.
[18] H.Y. Lee, W.S. Cho, S.M. Oh, H.D. Wiemhofer, W. Gopel, J. Electrochem. Soc. 142 (1995) 2659.
[19] S.P. Jiang, L.G. Love, Solid-State Ionics 138 (2001) 183.
[20] X.J. Chen, K.A. Khor, S.H. Chan, J. Power Sources 123 (2003) 17–25.
[21] W. Wang, S.P. Jiang, Solid-State Ionics 177 (2006) 1361.
[22] Y.D. Zhen, J. Li, S.P. Jiang, J. Power Sources 162 (2006) 1043.
[23] S.P. Jiang, Y.D. Zhen, S. Zhang, A.I.Y. Tok, P. Wu, J. Electrochem. Soc. 153 (2006) A2120.